Journal of Zhejiang University SCIENCE A
ISSN 1673-565X (Print); ISSN 1862-1775 (Online)
www.zju.edu.cn/jzus; www.springerlink.com
E-mail: jzus@zju.edu.cn

A relaxation scheme for a multi-class Lighthill-Whitham-Richards traffic flow model*

Jian-zhong CHEN†[1], Zhong-ke SHI[1], Yan-mei HU[2]

([1]*College of Automation, Northwestern Polytechnical University, Xi'an 710072, China*)

([2]*College of Science, Chang'an University, Xi'an 710064, China*)

†E-mail: jzhchen@nwpu.edu.cn

Received Nov. 30, 2008; Revision accepted Apr. 9, 2009; Crosschecked Oct. 18, 2009

Abstract: We present a high-resolution relaxation scheme for a multi-class Lighthill-Whitham-Richards (MCLWR) traffic flow model. This scheme is based on high-order reconstruction for spatial discretization and an implicit-explicit Runge-Kutta method for time integration. The resulting method retains the simplicity of the relaxation schemes. There is no need to involve Riemann solvers and characteristic decomposition. Even the computation of the eigenvalues is not required. This makes the scheme particularly well suited for the MCLWR model in which the analytical expressions of the eigenvalues are difficult to obtain for more than four classes of road users. The numerical results illustrate the effectiveness of the presented method.

Key words: Relaxation scheme, Multi-class LWR model, Traffic flow, CWENO reconstruction, Implicit-explicit Runge-Kutta
doi:10.1631/jzus.A0820829 **Document code:** A **CLC number:** O35; O24; U49

INTRODUCTION

Continuum traffic flow models have important applications such as traffic simulation and traffic control. The Lighthill-Whitham-Richards (LWR) model (Lighthill and Whitham, 1955; Richards, 1956) is the forerunner for all other continuum traffic flow models. The LWR model can describe a variety of real traffic phenomena such as shock formation. On the other hand, it fails to explain some important traffic phenomena such as hysteresis of traffic flow, the dispersion of platoon and the two-capacity phenomenon. To overcome deficiencies of the LWR model, much research was done in extending the LWR model recently. Zhang (2002) and Jiang *et al*. (2002) developed higher-order continuum models. Wong and Wong (2002) proposed a multi-class LWR model (MCLWR model) with heterogeneous drivers, which can remedy some deficiencies of the LWR model including the two-capacity phenomenon, hysteresis and platoon dispersion. For numerical methods, the Lax-Friedrichs scheme was employed to solve the MCLWR model (Wong and Wong, 2002). The Lax-Friedrichs scheme is only first-order accurate and yields a relatively poor resolution due to the excessive numerical dissipation. The Godunov scheme was also adopted to solve the LWR model (Lebacque, 1996) and higher-order model (Zhang, 2001). However, the Godunov scheme requires solving Riemann problems, which makes the scheme complicated and time-consuming. More recently, the high-order scheme has been applied to traffic flow models. The weighted essentially non-oscillatory (WENO) scheme was investigated for solving the MCLWR model with heterogeneous drivers (Zhang *et al*., 2003) and the MCLWR model on an inhomogeneous highway (Zhang *et al*., 2006). We attempted to use the high-resolution semi-discrete central-upwind scheme (Kurganov *et al*., 2001) for a two-class LWR model (Chen *et al*., 2007). One advantage of the high-order schemes is that they reduce the excessive numerical dissipation and give sharper resolution of the shocks

* Project supported by the Aoxiang Project and the Scientific and Technological Innovation Foundation of Northwestern Polytechnical University, China (No. 2007KJ01011)

and rarefactions. Moreover, high-order schemes need a relatively small number of grid points to resolve the problems in which solutions contain rich smooth region structures.

In this paper we focus on another type of shock-capturing scheme, the so-called 'high-resolution relaxation schemes' first proposed by Jin and Xin (1995). In contrast with upwind schemes such as the Godunov scheme, relaxation schemes require neither Riemann solvers nor the computation of Jacobians. In fact, even the computation of the eigenvalues can be avoided. We need only rough estimate of the upper boundary of the maximum of absolute eigenvalues. These features make the relaxation schemes suitable for those systems where the Riemann problem is difficult to solve or when there is no possibility to perform analytical expression for the eigenvalues of the Jacobians. The MCLWR model is a case of these systems. For this model, the analytical expressions of the eigenvalues are difficult to obtain for more than four classes of road users.

Recently, Banda and Seaïd (2005) proposed a general framework to generalize the relaxation schemes to higher orders of accuracy and developed a third-order scheme for hyperbolic systems of conservation laws. The main idea is to apply higher-order reconstructions for spatial discretization. This idea had been extended to numerical solution of coupled convection-radiation systems (Banda *et al*., 2007), Hamilton-Jacobi equations (Banda and Seaïd, 2006), shallow water equation (Seaïd, 2004) and hyperbolic systems of conservation laws (Chen and Shi, 2006; Banda and Seaïd, 2007). Along this line, this paper presents a high-resolution relaxation scheme for solving the MCLWR traffic flow model. This scheme is based on combining a fourth-order central WENO (CWENO) reconstruction (Levy *et al*., 1999) for spatial discretization with an implicit-explicit method for time discretization.

THE MULTI-CLASS LIGHTHILL-WHITHAM-RICHARDS MODEL

In this section, we recall the MCLWR model introduced by Wong and Wong (2002), which describes the characteristics of traffic flow of M classes of road users. Let $\rho_m(x,t)$ and $u_m(x,t)$ denote the density and speed of user class m, respectively. The MCLWR model can be written in the vector form as

$$\boldsymbol{U}_t + \boldsymbol{F}(\boldsymbol{U})_x = \boldsymbol{0}, \tag{1}$$

where $\boldsymbol{U}=[\rho_1, \rho_2, \ldots, \rho_M]^{\mathrm{T}}$ and $\boldsymbol{F}(\boldsymbol{U})=[\rho_1 u_1, \rho_2 u_2, \ldots, \rho_M u_M]^{\mathrm{T}}$. Introducing speed-density relationship, the system Eq.(1) is complete. The relationship presented by Wong and Wong (2002) has the form

$$u_m(x,t) = v_m(\rho),\ \forall m = 1,2,\cdots,M, \tag{2}$$

where $\rho = \sum_{m=1}^{M} \rho_m$ is the total density. From Eq.(2), we can see that this choice of speed of user class m is affected by all user classes.

For this model, an important issue is to verify the hyperbolicity since the analytical expressions of the eigenvalues are not available when M>4. This problem was validated numerically when M>2 (Wong and Wong, 2002; Zhang *et al*., 2003; Ngoduy and Liu, 2007). The theoretical discussion was introduced by Zhang *et al*.(2006). We assume that

$$v_1(\rho) < v_2(\rho) < \cdots < v_M(\rho). \tag{3}$$

According to Zhang *et al*.(2006), if $\boldsymbol{U}$ satisfies

$$\boldsymbol{U} \in D, D = \left\{ \boldsymbol{U} \middle| \rho_m > 0, m = 1,2,\cdots,M; \sum_{m=1}^{M} \rho_m < \rho_{\mathrm{jam}} \right\}, \tag{4}$$

where ρ_{jam} is the jam density, then the hyperbolicity of the system Eqs.(1) and (2) is guaranteed. Moreover, the eigenvalues $\{\lambda_m\}_{m=1}^{M}$ of the Jacobian $\boldsymbol{F}_{\boldsymbol{U}}$ satisfy

$$\begin{aligned} v_1 + \sum_{m=1}^{M} \rho_m \frac{\partial v_m}{\partial \rho} < \lambda_1 < v_1 < \lambda_2 < \cdots < v_{m-1} < \lambda_m \\ < v_m < \cdots < v_{M-1} < \lambda_M < v_M. \end{aligned} \tag{5}$$

In this context, we consider only the above cases.

NUMERICAL SCHEME

Based on the relaxation method proposed by Jin and Xin (1995), Eq.(1) can be approximated by the relaxation system

$$\begin{cases} \boldsymbol{U}_t + \boldsymbol{V}_x = \boldsymbol{0}, \\ \boldsymbol{V}_t + \boldsymbol{A}\boldsymbol{U}_x = -(\boldsymbol{V} - \boldsymbol{F}(\boldsymbol{U}))/\tau, \end{cases} \tag{6}$$

where $\boldsymbol{V}\in\mathbb{R}^M$, $\tau>0$ is the relaxation rate and $\boldsymbol{A}$=diag$\{a_1, a_2, \ldots, a_M\}$ is a positive diagonal matrix. According to the second equation in Eq.(6) we can obtain

$$\boldsymbol{V} = \boldsymbol{F}(\boldsymbol{U}) - \tau(\boldsymbol{V}_t + \boldsymbol{A}\boldsymbol{U}_x).$$

For small τ, applying a Chapman-Enskog expansion to Eq.(6), one can arrive at

$$\boldsymbol{U}_t + \boldsymbol{F}(\boldsymbol{U})_x = \tau((\boldsymbol{A} - \boldsymbol{F}'(\boldsymbol{U})^2)\boldsymbol{U}_x)_x.$$

It can be seen that the relaxation system Eq.(6) is NOT mathematically equivalent to the original problem when τ is kept finite. Under certain conditions the solution of Eq.(6) converges to the solution of the original problem as $\tau\to 0$. A necessary condition for such convergence is that a subcharacteristic condition

$$-\sqrt{a} \le \lambda \le \sqrt{a} \tag{7}$$

is satisfied. Here a=max$\{a_1, a_2, \ldots, a_M\}$ and λ is an arbitrary eigenvalue of $\boldsymbol{F}_{\boldsymbol{U}}$. The relaxation system of Eq.(6) has characteristic variables given by

$$\boldsymbol{V} \pm \boldsymbol{A}^{1/2}\boldsymbol{U}. \tag{8}$$

Without loss of generality, consider uniform spatial grid $x_j = j\Delta x$, $x_{j\pm\frac{1}{2}} = (j\pm 1/2)\Delta x$, where Δx is the uniform spatial step. The cell average of the variable $\boldsymbol{U}$ in $I_j = [x_{j-\frac{1}{2}}, x_{j+\frac{1}{2}}]$ at time t is denoted by $\boldsymbol{U}_j(t) = \frac{1}{\Delta x}\int_{I_j} \boldsymbol{U}(x,t)\mathrm{d}x$. The approximate point value of $\boldsymbol{U}$ at $(x_{j+\frac{1}{2}}, t)$ is denoted by $\boldsymbol{U}_{j+\frac{1}{2}}(t)$. Then the spatial discretization of Eq.(6) in conservation form can be written as

$$\begin{cases} \dfrac{\mathrm{d}}{\mathrm{d}t}\boldsymbol{U}_j + \dfrac{1}{\Delta x}(\boldsymbol{V}_{j+\frac{1}{2}} - \boldsymbol{V}_{j-\frac{1}{2}}) = \boldsymbol{0}, \\ \dfrac{\mathrm{d}}{\mathrm{d}t}\boldsymbol{V}_j + \dfrac{1}{\Delta x}\boldsymbol{A}(\boldsymbol{U}_{j+\frac{1}{2}} - \boldsymbol{U}_{j-\frac{1}{2}}) = -\dfrac{1}{\tau}(\boldsymbol{V}_j - \boldsymbol{F}(\boldsymbol{U})_j). \end{cases} \tag{9}$$

Assuming that the cell-averages $\{\boldsymbol{U}_j\}$ are known, our goal is to compute the cell point values $\boldsymbol{U}_{j+\frac{1}{2}}$ and $\boldsymbol{V}_{j+\frac{1}{2}}$ and the flux $\boldsymbol{F}(\boldsymbol{U})_j$. Following the notations introduced by Banda and Seaïd (2005), a piecewise reconstruction is built from the given cell-averages:

$$\tilde{\boldsymbol{U}}(x) = \sum\nolimits_j \boldsymbol{R}_j(x;\boldsymbol{U})\chi_j(x), \tag{10}$$

where χ_j is the characteristic function of the interval I_j and $\boldsymbol{R}_j(x;\boldsymbol{U})$ is a reconstruction polynomial defined in I_j. Given such a reconstruction, the point-values of $\tilde{\boldsymbol{U}}$ at the interface points are denoted by $\boldsymbol{U}^-_{j+\frac{1}{2}} = \boldsymbol{R}_j(x_{j+\frac{1}{2}};\boldsymbol{U})$ and $\boldsymbol{U}^+_{j-\frac{1}{2}} = \boldsymbol{R}_j(x_{j-\frac{1}{2}};\boldsymbol{U})$.

Reconstruction is a key step to spatial discretization. The original first- and second-order relaxation schemes (Jin and Xin, 1995) are based on piecewise-constant reconstruction and piecewise linear MUSCL (monotonic upstream schemes for conservation laws) reconstruction, respectively. The relaxation scheme (Seaïd, 2004; Banda and Seaïd, 2005; 2006; Banda *et al*., 2007) is based on the compact CWENO reconstruction (Levy *et al*., 2000). To improve resolution and reduce numerical dissipation, we use the fourth-order CWENO reconstruction (Levy *et al*., 1999). In each cell I_j, the kth component of this reconstruction is a convex combination of three quadratic polynomials, $P_l(x)$, l=j−1, j, j+1:

$$R_j(x;\boldsymbol{U}) = \omega^j_{j-1}P_{j-1}(x) + \omega^j_j P_j(x) + \omega^j_{j+1}P_{j+1}(x), \tag{11}$$

where the quadratic polynomials are

$$P_l(x) = \tilde{U}_l + \tilde{U}'_l(x - x_l) + \frac{1}{2}\tilde{U}''_l(x - x_l)^2,\ l=j-1, j, j+1. \tag{12}$$

Here $\tilde{U}''_l = (U_{l+1} - 2U_l + U_{l-1})/(\Delta x)^2$, $\tilde{U}_l = U_l - \tilde{U}''_l/24$, $\tilde{U}'_l = (U_{l+1} - U_{l-1})/(2\Delta x)$ and U is the kth component of $\boldsymbol{U}$. The weights ω^j_l are defined as

$$\omega^j_l = \frac{\alpha^j_l}{\alpha^j_{j-1} + \alpha^j_j + \alpha^j_{j+1}},\ \alpha^j_l = \frac{C_l}{(\varepsilon + \mathrm{IS}^j_l)^2}, \tag{13}$$

where C_{j-1}=C_{j+1}=3/16, C_j=5/8 and ε=10^{-6}. The smoothness indicators, IS_l, are given by

$$\begin{cases} \mathrm{IS}_{j-1}^{j}=\dfrac{13}{12}(U_{j-2}-2U_{j-1}+U_j)^2+\dfrac{1}{4}(U_{j-2}-4U_{j-1}+3U_j)^2, \\ \mathrm{IS}_{j}^{j}=\dfrac{13}{12}(U_{j-1}-2U_{j}+U_{j+1})^2+\dfrac{1}{4}(U_{j-1}-U_{j+1})^2, \\ \mathrm{IS}_{j+1}^{j}=\dfrac{13}{12}(U_{j}-2U_{j+1}+U_{j+2})^2+\dfrac{1}{4}(3U_j-4U_{j+1}+U_{j+2})^2. \end{cases} \tag{14}$$

In summary, the resulting reconstruction $R_j(x;U)$ can be written as

$$R_j(x;\boldsymbol{U})=\hat{U}_j+\hat{U}'_j(x-x_j)+\frac{1}{2}\hat{U}''_j(x-x_j)^2, \tag{15}$$

where

$$\begin{cases} \hat{U}_j=\omega_{j-1}^{j}\left(\tilde{U}_{j-1}+h\tilde{U}'_{j-1}+\dfrac{1}{2}h^2\tilde{U}''_{j-1}\right)+\omega_j^j\tilde{U}_j \\ \qquad +\omega_{j+1}^{j}\left(\tilde{U}_{j+1}-h\tilde{U}'_{j+1}+\dfrac{1}{2}h^2\tilde{U}''_{j+1}\right), \\ \hat{U}'_j=\omega_{j-1}^{j}(\tilde{U}'_{j-1}+h\tilde{U}''_{j-1})+\omega_j^j\tilde{U}'_j+\omega_{j+1}^{j}(\tilde{U}'_{j+1}-h\tilde{U}''_{j+1}), \\ \hat{U}''_j=\omega_{j-1}^{j}\tilde{U}''_{j-1}+\omega_j^j\tilde{U}''_j+\omega_{j+1}^{j}\tilde{U}''_{j+1}. \end{cases} \tag{16}$$

Then, the kth components of $\boldsymbol{V}\pm\boldsymbol{A}^{1/2}\boldsymbol{U}$ are discretized by

$$\begin{cases} (V+\sqrt{a_k}U)_{j+\frac{1}{2}}=R_j(x_{j+\frac{1}{2}};\boldsymbol{V}+\sqrt{a_k}\boldsymbol{U}), \\ (V-\sqrt{a_k}U)_{j+\frac{1}{2}}=R_{j+1}(x_{j+\frac{1}{2}};\boldsymbol{V}-\sqrt{a_k}\boldsymbol{U}), \end{cases} \tag{17}$$

where V is the kth component of $\boldsymbol{V}$. The point values can be calculated directly:

$$\begin{cases} U_{j+\frac{1}{2}}=\dfrac{1}{2\sqrt{a_k}}\left[R_j(x_{j+\frac{1}{2}};\boldsymbol{V}+\sqrt{a_k}\boldsymbol{U})-R_{j+1}(x_{j+\frac{1}{2}};\boldsymbol{V}-\sqrt{a_k}\boldsymbol{U})\right], \\ V_{j+\frac{1}{2}}=\dfrac{1}{2}\left[R_j(x_{j+\frac{1}{2}};\boldsymbol{V}+\sqrt{a_k}\boldsymbol{U})+R_{j+1}(x_{j+\frac{1}{2}};\boldsymbol{V}-\sqrt{a_k}\boldsymbol{U})\right]. \end{cases} \tag{18}$$

Here $U_{j+\frac{1}{2}}$ and $V_{j+\frac{1}{2}}$ are the kth component of $\boldsymbol{U}_{j+\frac{1}{2}}$ and $\boldsymbol{V}_{j+\frac{1}{2}}$, respectively.

The flux $\boldsymbol{F}(\boldsymbol{U})_j$ is approximated by Simpson's quadrature, yielding

$$F(U)_j=\frac{1}{6}\left(F(U_{j+\frac{1}{2}})+4F(U_j)+F(U_{j-\frac{1}{2}})\right). \tag{19}$$

Here $F(U)_j$ is the kth component of $\boldsymbol{F}(\boldsymbol{U})_j$.

The time discretization of the semi-discrete relaxation scheme is implemented using an implicit-explicit (IMEX) Runge-Kutta scheme (Ascher *et al*., 1997). The main advantage of this scheme is that the source terms are discretized by a diagonally implicit Runge-Kutta method and the convection terms are discretized by an explicit Runge-Kutta method. The semi-discrete formulation Eq.(9) is rewritten in common ordinary differential equations form:

$$\frac{\mathrm{d}\boldsymbol{Y}}{\mathrm{d}t}=\boldsymbol{L}(\boldsymbol{Y})-\frac{1}{\tau}\tilde{\boldsymbol{L}}(\boldsymbol{Y}), \tag{20}$$

where

$$\boldsymbol{Y}=\begin{pmatrix}\boldsymbol{U}_j\\ \boldsymbol{V}_j\end{pmatrix},\ \boldsymbol{L}(\boldsymbol{Y})=\begin{pmatrix}-D_x\boldsymbol{V}_j\\ -\boldsymbol{A}D_x\boldsymbol{U}_j\end{pmatrix},\ \tilde{\boldsymbol{L}}(\boldsymbol{Y})=\begin{pmatrix}\boldsymbol{0}\\ \boldsymbol{V}_j-\boldsymbol{F}(\boldsymbol{U})_j\end{pmatrix}. \tag{21}$$

Here $D_x\boldsymbol{V}_j=(\boldsymbol{V}_{j+\frac{1}{2}}-\boldsymbol{V}_{j-\frac{1}{2}})/\Delta x$. When applied to system Eq.(20), the IMEX scheme can be written as

$$\begin{cases} \boldsymbol{K}_l=\boldsymbol{Y}^n+\Delta t\sum\limits_{m=1}^{l-1}\bar{c}_{lm}\boldsymbol{L}(\boldsymbol{K}_m)-\dfrac{\Delta t}{\tau}\sum\limits_{m=1}^{s}c_{lm}\tilde{\boldsymbol{L}}(\boldsymbol{K}_m),\ l=1,2,\cdots,s, \\ \boldsymbol{Y}^{n+1}=\boldsymbol{Y}^n+\Delta t\sum\limits_{l=1}^{s}\bar{d}_l\boldsymbol{L}(\boldsymbol{K}_l)-\dfrac{\Delta t}{\tau}\sum\limits_{l=1}^{s}d_l\tilde{\boldsymbol{L}}(\boldsymbol{K}_l), \end{cases} \tag{22}$$

where $\bar{d}_l$ and d_l are the lth component of the s-vectors $\bar{\boldsymbol{d}}$ and $\boldsymbol{d}$, respectively, $\boldsymbol{Y}^n$ denotes the approximate solution at time $t^n=n\Delta t$, and $\boldsymbol{K}_l$ represents the intermediate result. The $s\times s$ matrices $\bar{\boldsymbol{C}}=(\bar{c}_{lm})$ and $\boldsymbol{C}=(c_{lm})$ are selected such that the resulting scheme is explicit in $\boldsymbol{L}$, and implicit in $\tilde{\boldsymbol{L}}$. Using the Butcher notation, IMEX schemes can be expressed by a double tableau

$$\begin{array}{c|c}\bar{\boldsymbol{e}}&\bar{\boldsymbol{C}}\\ \hline &\bar{\boldsymbol{d}}^{\mathrm{T}}\end{array},\quad \begin{array}{c|c}\boldsymbol{e}&\boldsymbol{C}\\ \hline &\boldsymbol{d}^{\mathrm{T}}\end{array},$$

where $\bar{\boldsymbol{e}}$ and $\boldsymbol{e}$ are the s-vectors used in the context of non-autonomous systems. The left and right tables are associated with the explicit and implicit Runge-Kutta methods, respectively. A third-order IMEX scheme (Ascher *et al*., 1997) is used in this study. The corresponding double tableau is

$$\begin{array}{c|cccc} 0 & 0 & 0 & 0 \\ \gamma & \gamma & 0 & 0 \\ 1-\gamma & \gamma-1 & 2-2\gamma & 0 \\ \hline & 0 & 1/2 & 1/2 \end{array}, \quad \begin{array}{c|ccc} 0 & 0 & 0 & 0 \\ \gamma & 0 & \gamma & 0 \\ 1-\gamma & 0 & 1-2\gamma & \gamma \\ \hline & 0 & 1/2 & 1/2 \end{array}, \tag{23}$$

where $\gamma = (3+\sqrt{3})/6$.

The Courant-Friedrichs-Lewy (CFL) number is defined by

$$\mathrm{CFL} = \max_m \left\{ \sqrt{a_m} \frac{\Delta t}{\Delta x} \right\} \le 1. \tag{24}$$

The parameters a_m for $1 \le m \le M$ are chosen according to inequality Eq.(5). A simple choice is to take $\sqrt{a_m} = \max\left(\left| v_1 + \sum_{m=1}^{M} \rho_m \frac{\partial v_m}{\partial \rho} \right|, |v_M| \right)$ for $1 \le m \le M$. Another more precise choice is to set $\sqrt{a_1} = \max\left(\left| v_1 + \sum_{m=1}^{M} \rho_m \frac{\partial v_m}{\partial \rho} \right|, |v_1| \right)$ and $\sqrt{a_m} = |v_m|$ for $2 \le m \le M$. Both choices satisfy the subcharacteristic condition Eq.(7). Other choices can be obtained as long as the condition Eq.(7) holds.

NUMERICAL EXAMPLES

In this section, we present some numerical tests to validate the performance of the presented relaxation scheme for the MCLWR model. We use N to denote the number of grid points in our computations. The relaxation rate τ was set to 10^{-6}.

Boundary conditions

We first considered the boundary conditions for $\boldsymbol{U}$ in our computations. For periodic boundary conditions, the values of ghost points were directly set by using periodic conditions. If constant density is assumed on the left boundary, we simply set the left ghost-cell values to be this constant. Except for the above two cases, we use fourth-order extrapolation to assign the values in all necessary ghost points. Following Jin and Xin (1995), the choice of the boundary conditions for $\boldsymbol{V}$ is consistent with the local equilibrium $\boldsymbol{V}=\boldsymbol{F}(\boldsymbol{U})$ in order to avoid the boundary layer.

Test 1: Comparison of Runge-Kutta methods

The IMEX method was used for time integration. Using a test introduced by LeVeque (2002), we compared the two kinds of Runge-Kutta methods—the third-order IMEX method and total variation diminishing (TVD) Runge-Kutta (Shu and Osher, 1988). Consider the linear equation

$$u_t + u_x = -(1-x)u, \quad x \in [0,1]$$

with initial data consisting of a Gaussian pulse centered at x=0.25. The spatial discretization was obtained by the scheme proposed by Kurganov *et al*. (2001). The source term was approximated by the midpoint rule. A comparison of the CPU time at t=0.5 is presented in Table 1.

Table 1 CPU time for different Runge-Kutta methods in Test 1*

Time discretization method	CPU time (s)	
	N=2000	N=4000
Third-order IMEX	4.20	16.51
Third-order TVD Runge-Kutta	3.94	15.66

* On a Pentium IV 2.4 GHz PC with 512 MB RAM. N: number of grid points

Test 2: Two classes of road users

In this subsection, we verify our scheme on a model that involves two classes of road users. The relationships Eq.(2) are defined as follows:

$$u_1 = v_1(\rho) = u_{\mathrm{f}1}(1-\rho/\rho_n), u_2 = v_2(\rho) = u_{\mathrm{f}2}(1-\rho/\rho_n), \tag{25}$$

where ρ_n is maximal density and $u_{\mathrm{f}1}$ and $u_{\mathrm{f}2}$ are the free flow velocity for Class 1 and Class 2 traffic, respectively. The variables of space, time, density and velocity are scaled by L, t, ρ_n and u_{f}, where L is the length of the road, t is computational time and $u_{\mathrm{f}}=\max(u_{\mathrm{f}1}, u_{\mathrm{f}2})$. Moreover, a variable is also non-dimensional if it is not followed by its unit. In this test, we took $\sqrt{a_1} = \sqrt{a_2} = \max\left(\left| v_1 + \sum_{m=1}^{2} \rho_m \frac{\partial v_m}{\partial \rho} \right|, |v_2| \right)$. We studied the performance of our method using three test cases. The test cases 2 and 3 were presented by Zhang *et al.*(2005).

Case 1 (Accuracy test) The parameters used were $L=10^4$ m, u_{f1}=10 m/s and u_{f2}=20 m/s. The smooth initial data were given by $\rho_1(x,0)=0.2+0.2\sin(2\pi x)$, $\rho_2(x,0)=0.3-0.2\sin(2\pi x)$, with periodic boundary conditions. To avoid discontinuities in the solution, we computed the solution at time t=0.05. This test case was used to check the convergence rate. Since the exact solution is not available for this case, we used our method with 3200 grid points to compute a reference solution and it was assumed as the exact solution in calculating the numerical errors. Since the third-order IMEX scheme was used for temporal discretization, the time step was chosen to be $\Delta t = O(\Delta x^{4/3})$ to guarantee the accuracy in time. The errors and numerical orders of accuracy are shown in Table 2.

Table 2 Accuracy test for the two classes of road users, at t=0.05

N	L^∞-error	Order	L^1-error	Order
100	0.1192E-3	−	0.6061E-4	−
200	0.9097E-5	3.71	0.4660E-5	3.70
400	0.6239E-6	3.87	0.3183E-6	3.87
800	0.3529E-7	4.14	0.1853E-7	4.10

N: number of grid points

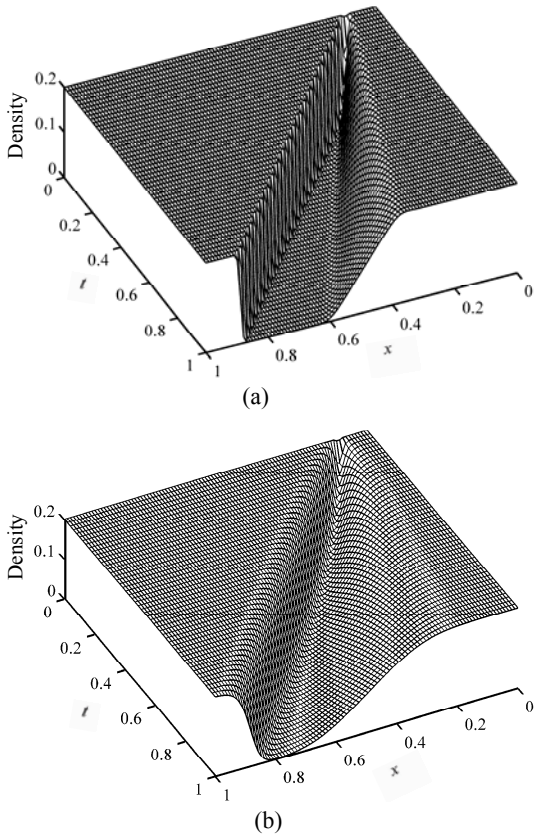

Fig.1 Separation of the two traffic flows, total density
(a) RS-CWENO scheme; (b) Lax-Friedrichs scheme

Case 2 (Separation of the two traffic flows) The parameters used were L=8000 m, T=400 s, Δx=80 m, Δt=0.4 s, u_{f1}=10 m/s and u_{f2}=20 m/s. The initial conditions were $\boldsymbol{U}(x,0)=\begin{cases}(0.2,0), & x<0.1,\\ (0,0.2), & x>0.1.\end{cases}$ In this case, Class 1 drivers cannot keep up with Class 2 drivers since $u_2>u_{f1}$. This led to a vacuum region between Class 1 and Class 2 traffic. The test had a solution consisting of a right shock, a constant region and a left rarefaction. Here and below, the scheme presented in this paper is abbreviated to the RS-CWENO scheme. Fig.1a shows the solution computed by the RS-CWENO scheme. To illustrate the advantage of using high-order schemes, the numerical results obtained by the first-order Lax-Friedrichs scheme are shown in Fig.1b.

Case 3 (Mixture of the two traffic flows) In this case, the parameters were chosen as follows: L=6000 m, T=400 s, Δx=60 m, Δt=0.4 s, u_{f1}=14 m/s and u_{f2}=20 m/s. The initial data were $\boldsymbol{U}(x,0)=\begin{cases}(0,0.4), & x<0.1,\\ (0.4,0), & x>0.1.\end{cases}$ In this test Class 2 traffic mixed in Class 1 traffic, which led to the increase of the total density. Its solution contained a shock, a constant region and a rarefaction. Fig.2a shows the total density computed by the RS-CWENO scheme. For comparison, the first-order relaxation scheme (Jin and Xin, 1995) was also adopted to compute the total density in this test. The corresponding results are presented in Fig.2b.

In summary, we have compared the high-order relaxation scheme with the low-order Lax-Friedrichs scheme and relaxation scheme in cases 2 and 3. These comparisons showed the advantage of the high-order scheme, i.e., higher shock resolution and smaller numerical dissipation.

Test 3: Nine classes of road users

We considered an example of nine classes of road users studied by Wong and Wong (2002) to illustrate the capability of the MCLWR model in properly describing platoon dispersion. It has also been computed to verify the convergence of the WENO scheme for the MCLWR model (Zhang *et al*., 2003). Consider a

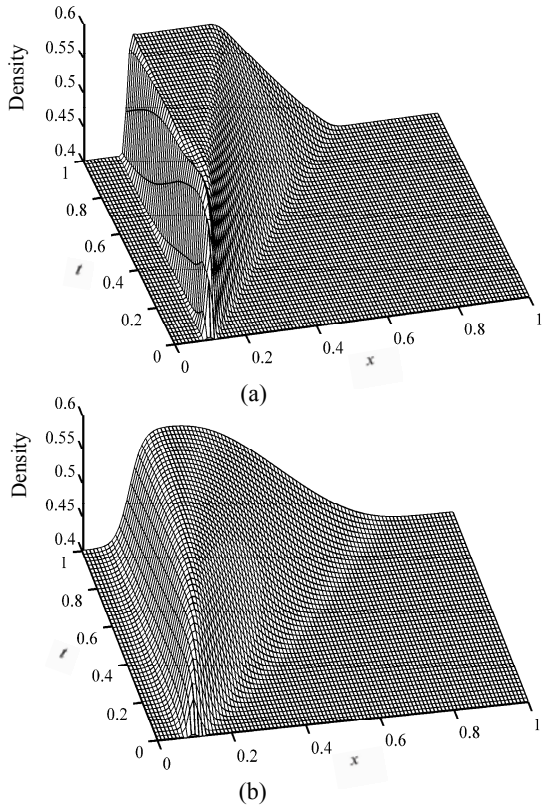

Fig.2 Mixture of the two traffic flows, total density
(a) RS-CWENO scheme; (b) First-order relaxation scheme

2 km long highway. On the left boundary a constant density of 0 veh./km was imposed, while on the right boundary a free outflow condition was assumed. The speed-density relationship modified from Drake *et al*.(1967),

$$u_m = v_m(\rho) = u_{fm} \exp(-(\rho/\rho_0)^2/2),\ m = 1,2,\cdots,9, \quad (26)$$

was assumed for all user classes, where u_{fm} is the free flow speed of user class m and ρ_0 is a common parameter for all user classes. The free-flowing speeds were set as 60.0, 67.5, 75.0, …, 120.0 km/h. The distribution for these user classes is presented in Fig.3. The optimal density ρ_0 was set to 50 veh./km. In this test we took $\sqrt{a_9} = \max\left(\left|v_1 + \sum_{m=1}^{M} \rho_m \frac{\partial v_m}{\partial \rho}\right|, |v_9|\right)$, $\sqrt{a_m} = |v_3|$ for m=1, 2, …, 8 and CFL=0.475.

Case 1 (Non-congested traffic regime) The initial platoon in the non-congested traffic regime is shown in Fig.4. The maximum density was 40 veh./km, which is below the optimal density ρ_0=50 veh./km. The traffic regime was not congested. Using this test case, we compared the RS-CWENO scheme with the third-order scheme (Banda and Seaïd, 2005) and the second-order method with MUSCL reconstruction (Jin and Xin, 1995). Fig.5 contains a comparison between our method and the second-order relaxation scheme using different meshes. The output time was t=0.015 h. The solutions were plotted together with a reference solution, which was computed by the Lax-Friedrichs scheme with 25 600 grid points. Fig.6 gives the results computed by the RS-CWENO method and the third-order relaxation scheme at different times, using N=400 grid points. According to Zhang *et al*.(2003), there are nine small staircases relative to the nine user classes and these staircases are actually shocks in different characteristic fields. From Figs.5d and 6a, we can see that there was a clear improvement in resolution when using the RS-CWENO scheme. The second- and third-order scheme missed these staircases due to the excessive numerical dissipation. These comparisons showed that the solutions computed by the RS-CWENO scheme were more accurate than the corresponding solutions of the second- and third-order relaxation scheme. Table 3 presents the CPU time for different relaxation schemes at t=0.015 h, using 200 and 400 grid points. Although the per grid cell cost of the RS-CWENO scheme was higher than that of the second- and third-order scheme, it was still more efficient.

Table 3 CPU time for different relaxation schemes for non-congested regime at t=0.015 h

Scheme	CPU time (s)	
	N=200	N=400
Second-order	2.08	8.45
Third-order	4.47	17.60
RS-CWENO	5.31	21.00

N: number of grid points

Case 2 (Congested traffic regime) The initial platoon in the congested traffic regime is shown in Fig.7a. It had a maximum density value of 120 veh./km, which is much larger than the optimal density ρ_0=50 veh./km. The traffic regime was congested. Fig.7b shows the total density as a function of spatial location at five different times, using 400 grid points.

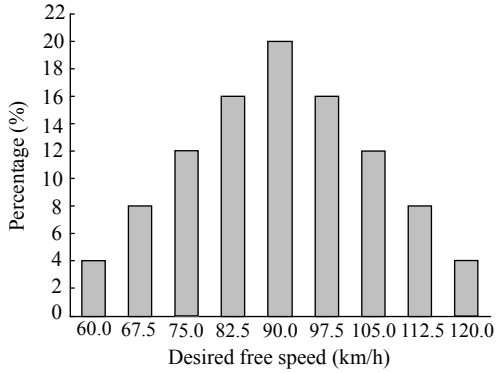

Fig.3 Nine classes of road users: distribution of free speed

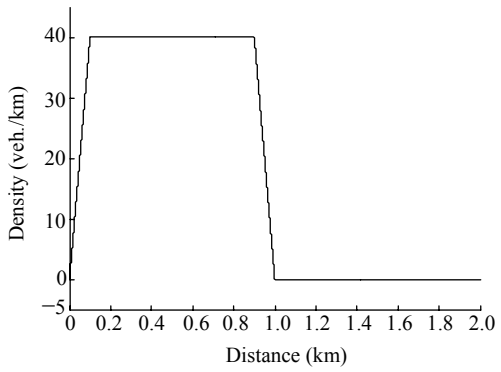

Fig.4 Non-congested traffic regime: initial platoon

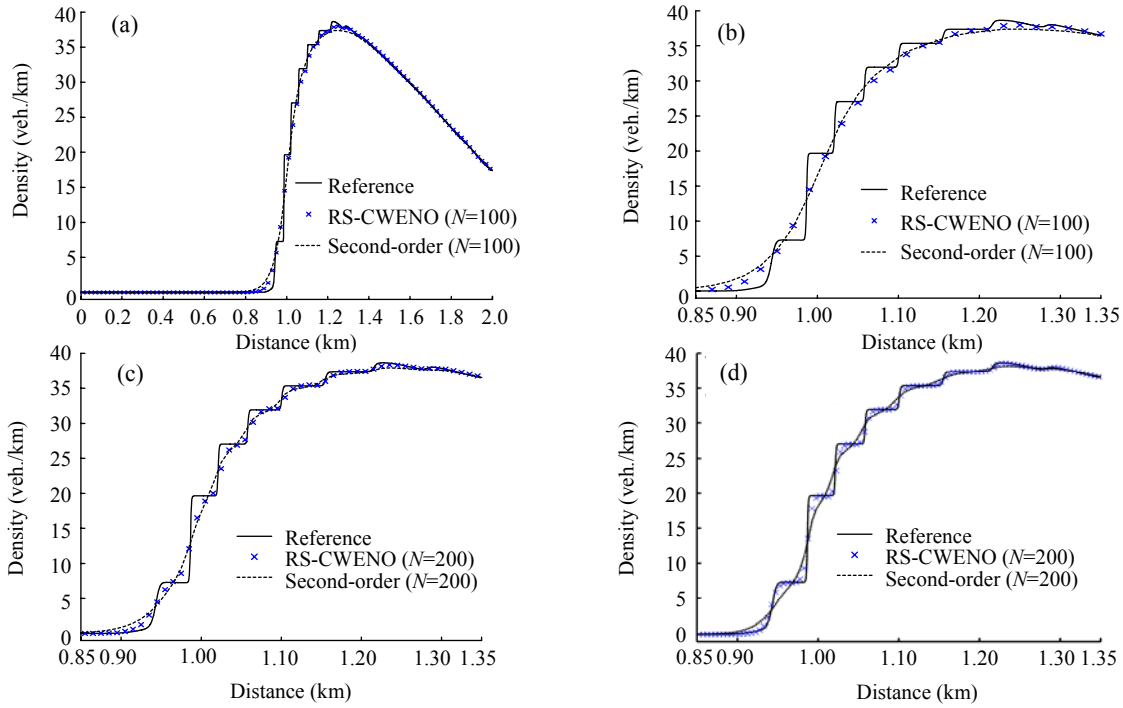

Fig.5 Comparison of non-congested regime total density at t=0.015 h between the RS-CWENO method and second-order relaxation scheme using different meshes

(a) N=100; (b) Same as (a)—zoom at [0.85, 1.35]; (c) N=200, zoom at [0.85, 1.35]; (d) N=400, zoom at [0.85, 1.35]

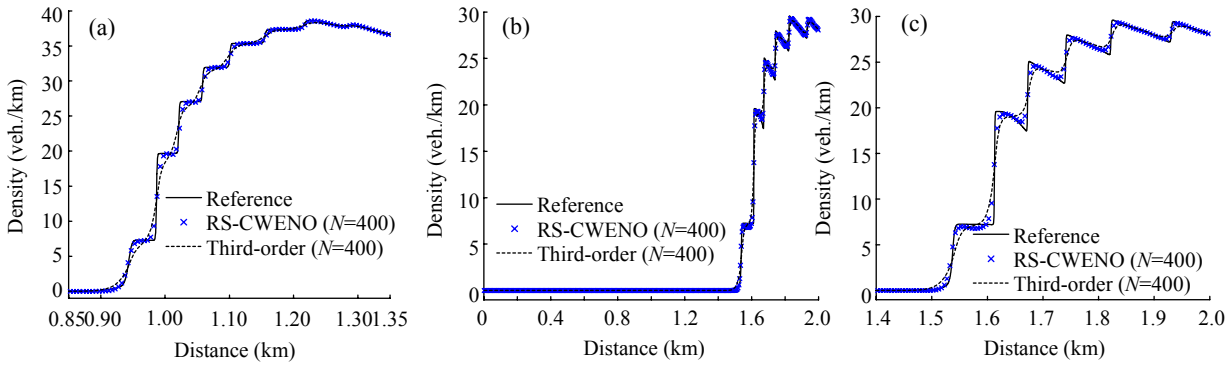

Fig.6 Comparison of non-congested regime total density between the RS-CWENO method and third-order relaxation scheme at different times

(a) t=0.015 h, N=400, zoom at [0.85, 1.35]; (b) t=0.025 h, N=400; (c) Same as (b)—zoom at [1.4, 2.0]

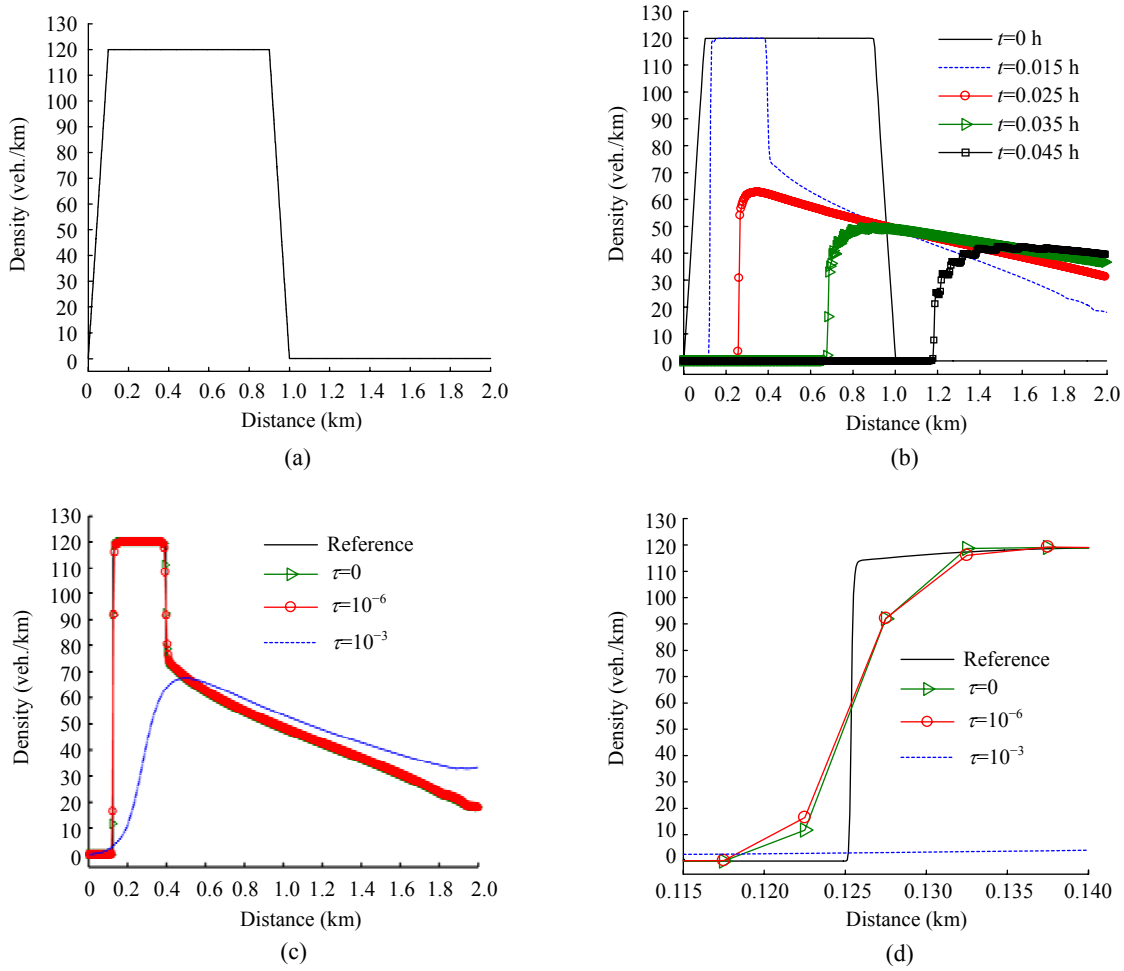

Fig.7 Congested regime

(a) Initial platoon; (b) Total density as a function of spatial location, for t=0, 0.015, 0.025, 0.035, 0.045 h; (c) t=0.015 h, N=400, total density using different relaxation rates; (d) Same as (c)—zoom at [0.115, 0.140]

This case was also used to test the influence of the relaxation rate, τ. Figs.7c and 7d compare the numerical results using 400 grid points for τ=0, 10^{-6}, 10^{-3}. We would like to mention that one arrived at the relaxed scheme when τ=0. The time discretization of the relaxed scheme can be achieved by using the explicit scheme given by the left table in Eq.(23). The output time was t=0.015 h. The reference solution was computed by the Lax-Friedrichs scheme with 25600 grid points. The computed total density when τ=10^{-3} deviated from the reference solution. The result obtained by the relaxed scheme (τ=0) was only slightly better than that computed by the relaxation scheme with τ=10^{-6}. Both results showed good agreement with the reference solution.

CONCLUSION

In this paper we have implemented a high-resolution relaxation scheme for an MCLWR traffic flow model. The new method is based on a fourth-order CWENO reconstruction and an implicit-explicit Runge-Kutta method. It has been tested on two examples. The obtained results showed that introducing a fourth-order CWENO reconstruction into the relaxation framework improves the resolution dramatically. The results also suggested that relaxation schemes can be of further consideration to implement and apply to other traffic flow models. We would like to point out that the relaxation scheme is just a representative of high-resolution schemes that

have the advantage of avoiding the expression of the eigenvalues. The schemes based on Lax-Friedrichs flux also have this advantage and may perform well in the MCLWR model, but we do not study them in this study.

References

Ascher, U.M., Ruuth, S.J., Spiteri, R.J., 1997. Implicit-explicit Runge-Kutta methods for time-dependent partial differential equations. *Appl. Numer. Math.*, **25**(2-3):151-167. [doi:10.1016/S0168-9274(97)00056-1]

Banda, M., Seaïd, M., 2006. Non-oscillatory methods for relaxation approximation of Hamilton-Jacobi equations. *Appl. Math. Comput.*, **183**(1):170-1183. [doi:10.1016/j.amc.2006.05.066]

Banda, M., Seaïd, M., 2007. Relaxation WENO schemes for multidimensional hyperbolic systems of conservation laws. *Numer. Methods Part. Diff. Equat.*, **23**(5):1211-1234. [doi:10.1002/num.20218]

Banda, M.K., Seaïd, M., 2005. Higher-order relaxation schemes for hyperbolic systems of conservation laws. *J. Numer. Math.*, **13**(3):171-196. [doi:10.1515/156939505774286102]

Banda, M.K., Klar, A., Seaïd, M., 2007. A lattice-Boltzmann relaxation scheme for coupled convection-radiation systems. *J. Comput. Phys.*, **226**(2):1408-1431. [doi:10.1016/j.jcp.2007.05.030]

Chen, J.Z., Shi, Z.K., 2006. Application of a fourth-order relaxation scheme to hyperbolic systems of conservation laws. *Acta Mech. Sin.*, **22**(1):84-92. [doi:10.1007/s10409-005-0079-x]

Chen, J.Z., Shi, Z.K., Hu, Y.M., 2007. Numerical Solution of a Two-class LWR Traffic Flow Model by High-resolution Central-upwind Scheme. Proc. 7th Int. Conf. on Computational Science, p.17-24. [doi:10.1007/978-3-540-72584-8_3]

Drake, J.S., Schofer, J.L., May, A.D., 1967. A statistical analysis of speed density hypothesis. *Highway Res. Rec.*, **154**:53-87.

Jiang, R., Wu, Q.S., Zhu, Z.J., 2002. A new continuum model for traffic flow and numerical tests. *Transp. Res. B*, **36**(5):405-419. [doi:10.1016/S0191-2615(01)00010-8]

Jin, S., Xin, Z., 1995. The relaxation schemes for systems of conservation laws in arbitrary space dimensions. *Commun. Pure Appl. Math.*, **48**(3):235-276. [doi:10.1002/cpa.3160480303]

Kurganov, A., Nolle, S., Petrova, G., 2001. Semi-discrete central-upwind scheme for hyperbolic conservation laws and Hamilton-Jacobi equations. *SIAM J. Sci. Comput.*, **23**(3):707-740. [doi:10.1137/S1064827500373413]

Lebacque, J.P., 1996. The Godunov Scheme and What It Means for First Order Traffic Flow Models. Proc. 13th Int. Symp. on Transportation and Traffic Theory, p.647-677.

LeVeque, R.J., 2002. Finite Volume Methods for Hyperbolic Problems. Cambridge University Press, Cambridge, UK, p.378-388.

Levy, D., Puppo, G., Russo, G., 1999. Central WENO schemes for hyperbolic systems of conservation laws. *ESAIM Math. Model. Numer. Anal.*, **33**(3):547-571. [doi:10.1051/m2an:1999152]

Levy, D., Puppo, G., Russo, G., 2000. Compact central WENO schemes for multidimensional conservation laws. *SIAM J. Sci. Comput.*, **22**(2):656-672. [doi:10.1137/S1064827599359461]

Lighthill, M.J., Whitham, G.B., 1955. On kinematic waves (II): a theory of traffic flow on long crowed roads. *Proc. R. Soc. Ser. A*, **229**(1178):317-345. [doi:10.1098/rspa.1955.0089]

Ngoduy, D., Liu, R., 2007. Multiclass first-order simulation model to explain non-linear traffic phenomena. *Phys. A*, **385**(2):667-682. [doi:10.1016/j.physa.2007.07.041]

Richards, P.I., 1956. Shock waves on the highway. *Oper. Res.*, **4**(1):42-51. [doi:10.1287/opre.4.1.42]

Seaïd, M., 2004. Non-oscillatory relaxation methods for the shallow water equations in one and two space dimensions. *Int. J. Numer. Methods Fluids*, **46**(5):457-484. [doi:10.1002/fld.766]

Shu, C.W., Osher, S., 1988. Effient implementation of essentially non-oscillatory shock-capturing schemes. *J. Comput. Phys.*, **77**(2):439-471. [doi:10.1016/0021-9991(88)90177-5]

Wong, G.C.K., Wong, S.C., 2002. A multi-class traffic flow model: an extension of LWR model with heterogeneous drivers. *Transp. Res. A*, **36**(9):827-841. [doi:10.1016/S0965-8564(01)00042-8]

Zhang, H.M., 2001. A finite difference approximation of a non-equilibrium traffic flow model. *Transp. Res. B*, **35**(4):337-365. [doi:10.1016/S0191-2615(99)00054-5]

Zhang, H.M., 2002. A non-equilibrium traffic model devoid of gas-like behavior. *Transp. Res. B*, **36**(3):275-290. [doi:10.1016/S0191-2615(00)00050-3]

Zhang, M.P., Shu, C.W., Wong, G.C.K., Wong, S.C., 2003. A weighted essentially non-oscillatory numerical scheme for a multi-class Lighthill-Whitham-Richards traffic flow model. *J. Comput. Phys.*, **191**(2):639-659. [doi:10.1016/S0021-9991(03)00344-9]

Zhang, P., Liu, R.X., Dai, S.Q., 2005. Theoretical analysis and numerical simulation on a two-phase traffic flow LWR model. *J. Univ. Sci. Technol. China*, **35**(1):1-11 (in Chinese).

Zhang, P., Wong, S.C., Shu, C.W., 2006. A weighted essentially non-oscillatory numerical scheme for a multi-class traffic flow model on an inhomogeneous highway. *J. Comput. Phys.*, **212**(2):739-756. [doi:10.1016/j.jcp.2005.07.019]